Supplementary Information: Co-encapsulation of Organic Polymers and Inorganic Superparamagnetic Iron Oxide Colloidal Crystals Requires Matched Diffusion Time Scales

Brian K. Wilson[1] and Robert K. Prud'homme[1,*]

[1] Department of Chemical and Biological Engineering, Princeton University, Princeton, NJ, USA 08544

[*]Corresponding author

Email: prudhomm@princeton.edu
Telephone: 609-258-4577
Address: A301 Engineering Quadrangle,
Princeton University
41 Olden Street
Princeton, NJ 08544

Contents

S1. Measuring Nanoparticle Components by Ultraviolet-Visible (UV-Vis) Absorption

Iron oxide has a broad visible absorption spectrum as evidenced by its black color, even in dilute concentrations. However, small particles like the nanoparticles produced here scatter ultraviolet and visible light with shorter wavelengths scattered more strongly. This scattering (of a photon beam away from a detector in a UV-Vis measurement) produces an apparent absorption signal at wavelengths typically up to around 500 nm. The extinction coefficient of iron oxide, around 400 nm, is expected to be much higher than the effective extinction coefficient due to scattering from nanoparticles. Validating the contribution of both iron oxide loaded and polymer only species to the absorbance signal is important to understand the reliability of the measurement.

A400 measurements were taken of mixed dispersion of either iron oxide loaded nanoparticles or polymer-only nanoparticles, shown in Figure S1, all containing the usual 2%wt Hostasol Yellow 3G in poly(styrene) loading. The goal here is to establish a linear relationship between the concentration of each type of nanoparticle with the measured total absorbance. The simple addition of the concentration of the iron oxide loaded nanoparticles and polymer only nanoparticles (Figure S2, circles) produces widely spaced data, where increasing amounts of polymer-only nanoparticles produces only a small increase in absorbance (the horizontal bands correspond to the iron oxide nanoparticle concentration with only a small increase moving left to right) as evidenced by the vastly different extinction coefficients in Figure S1 (slope of each curve). Utilizing only the concentration of the iron oxide loaded nanoparticles (Figure S2, triangles) produces a more-linear fit but with points clearly dispersed vertically around the line of best fit, where the vertical displacement correlates with the polymer-only nanoparticle concentration. The best linearization is produced when using an extinction coefficient-weighted

linear combination of the iron oxide-loaded and polystyrene-only concentrations; however, the slope does not vary significantly between the iron oxide-only and weighted linear combination linear fits. This combination is described in Equation S1 below.

$$C_{effective} = C_{FeOx} + K \times C_{PS} \text{ where } K = \frac{\epsilon_{PS}}{\epsilon_{PS} + \epsilon_{FeOx}} \quad \text{(Eqn S1)}$$

When applying Eqn S1 to the data, slightly different K-values are calculated for the small and medium iron oxide colloids (large iron oxide colloids produce data nearly identical to the medium iron oxide colloids.) The K-ratio is 0.0536 for small primary colloids and 0.0362 for medium primary colloids; this can be interpreted as polymer-only nanoparticles having an A400 absorbance between 3% to 5% that of the iron oxide loaded nanoparticles. The A400 measurement can be used as a reliable indicator of iron oxide concentration, with a margin less than 5% for any fluctuations in polymer-only nanoparticle concentrations also in dispersion.

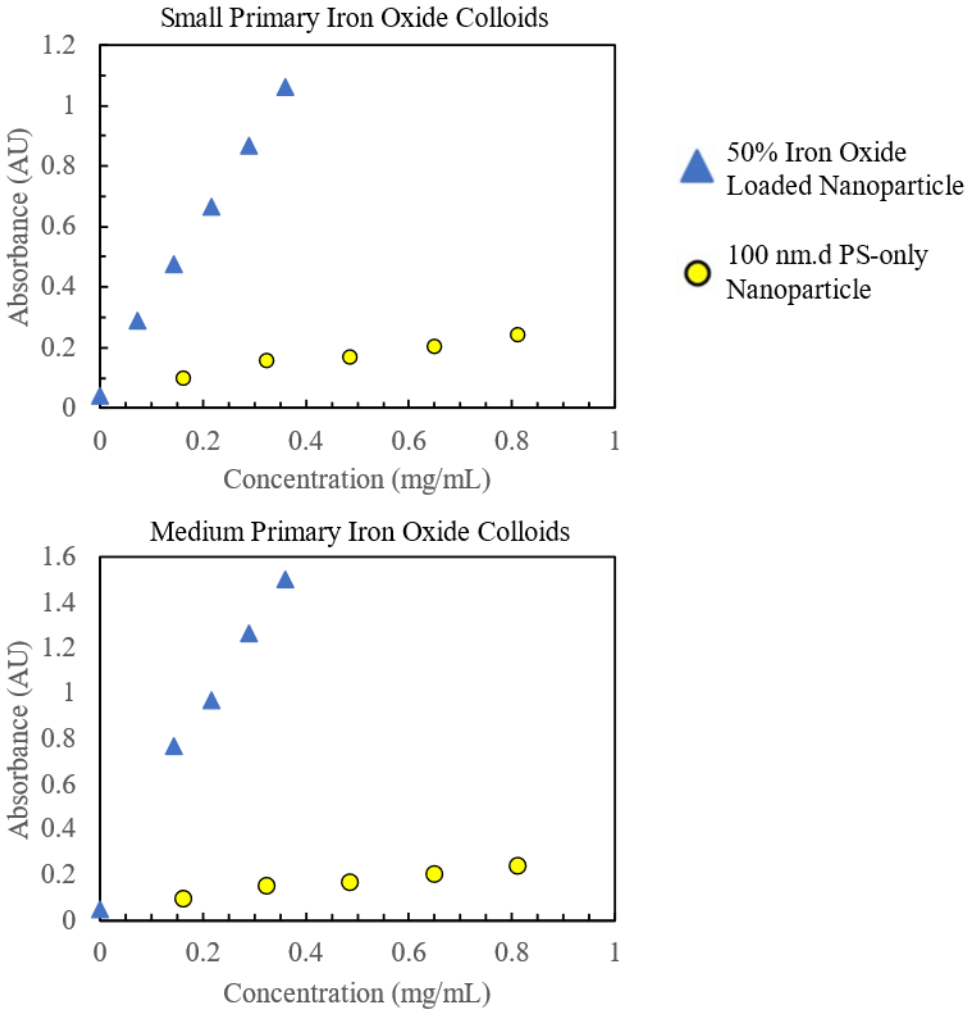

Figure S1. A400 measurements on mixed nanoparticle dispersions. 400 nm wavelength absorbance for 100 nm diameter nanoparticles containing iron oxide (triangles) or only poly(styrene) (circles) for both small and medium sized primary iron oxide colloids. The large iron oxide colloids produce a signal like the medium sized iron oxide.

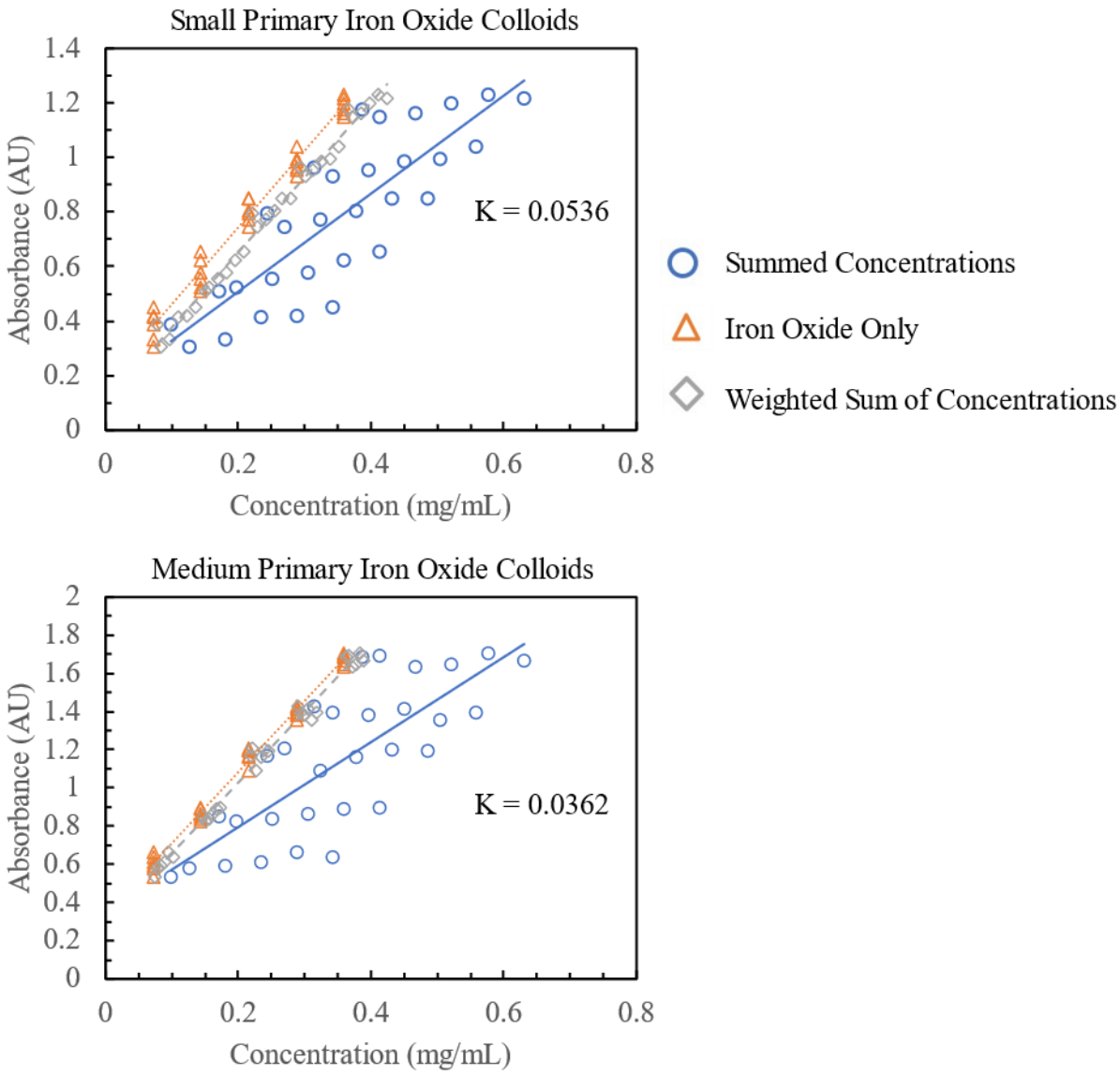

Figure S2. Concentration-weighting models for linearizing A400 measurements. 400 nm absorbance of combined iron oxide loaded nanoparticles and poly(styrene) only nanoparticles requires an absorption-weighted sum of the two nanoparticle species to produce a linear universal relationship between absorption and total particle concentration. Three different models for the total effective concentration of particles based on the A400 signal are plotted: simple addition of total solids concentration (circles), iron oxide loaded nanoparticles only (triangles), and a weighted sum (diamonds) where $C_{eff} = C_{FeOx} + K\ C_{PS\ only}$ (Eqn S.2). K-values (extinction coefficient ratio) are annotated on each plot.

S2. Characterization of Iron Oxide Primary Colloids by Thermogravimetric Analysis

The hydrophobic iron oxide oleate-coated primary colloids were characterized by TEM (for size, as shown in the main text as Figure 2) and by thermogravimetric analysis (TGA) using a TA Instruments (New Castle, DE) Q50 TGA for composition. Samples were heated in a nitrogen atmosphere with the following temperature program:

1. Isothermal for 1 minute. (Quantifies solvent evaporation for initial point correction if total concentration is a desirable parameter.)
2. Ramp at 25 °C/minute to 85 °C and then hold at 85 °C for 10 minutes. (Evaporates solvent to yield the total solids in the sample, iron oxide core plus oleate surface coating.)
3. Ramp at 25 °C/minute to 650 °C and then hold at 650 °C for 15 minutes. (Ramp above 350°C begins to evaporate oleate coating and residual solids at 650°C represents the iron oxide core only.)

The total density (ρ) of the different-size iron oxide species is calculated from a mass fraction weighted (x_i) linear combination of the bulk density of iron oxide (Fe_3O_4) and oleic acid (ρ_i) in Equation S2 below. The mass fraction composition of each iron oxide colloid species is determined from the thermograms by taking the ratio of the residual, iron oxide only, mass at 650 °C to the total dry colloids at 85 °C, as shown in Figures S3, S4, and S5.

$$\rho = \sum x_i \rho_i = x_{Iron\ Oxide}\rho_{Iron\ Oxide} + x_{Oleic\ Acid}\rho_{Oleic\ Acid} \quad \text{(Eqn S2)}$$

Table S1. Primary Iron Oxide Colloid Properties

ID	Average Diameter from TEM (nm)	Iron Oxide Composition (%wt of total colloid)	Calculated Average Density (mg/mL)
Small	5.5 ± 0.75	48.5 ± 0.67	1561
Medium	15.3 ± 1.2	62.4 ± 1.6	1984
Large	28.7 ± 3.2	81.0 ± 2.5	3106

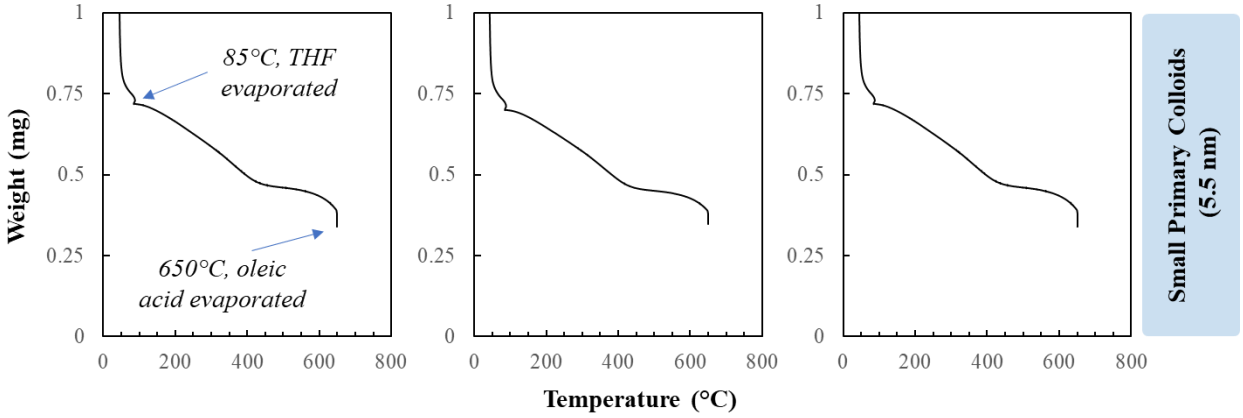

Figure S3. Thermogravimetric analysis of small (5.5 nm diameter, nm.d) primary oleate-coated iron oxide primary colloids. Samples are loaded as a dispersion in tetrahydrofuran, which is dried to yield total solids. The three curves are triplicate repeats.

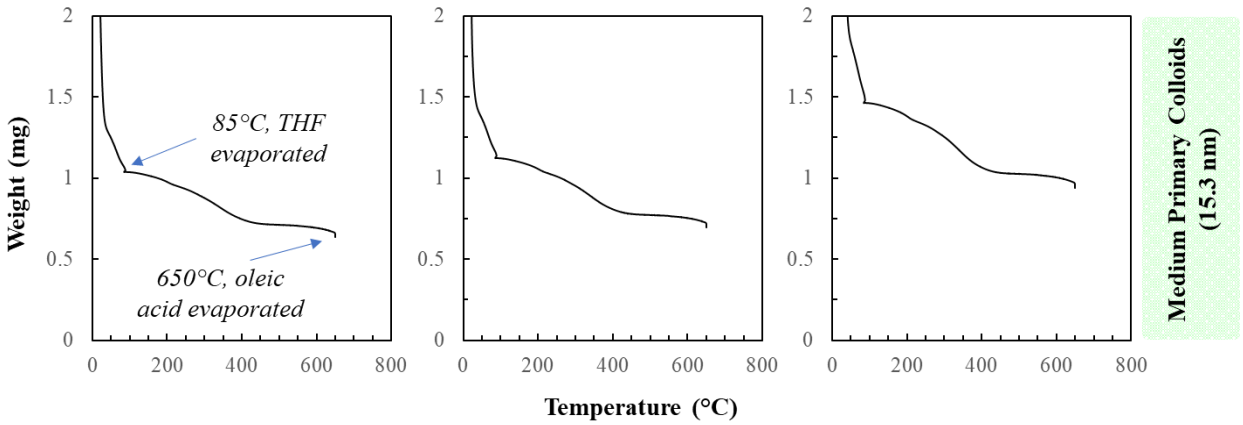

Figure S4. Thermogravimetric analysis of medium (15.3 nm.d) primary oleate-coated iron oxide primary colloids. Analyzed in the same way as in Figure S1.

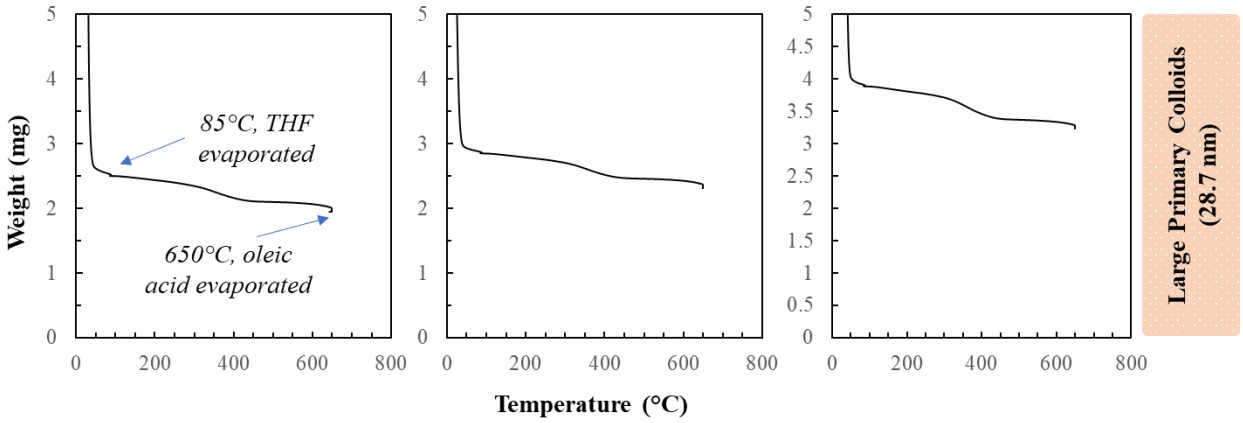

Figure S5. Thermogravimetric analysis of large (28.7 nm.d) primary oleate-coated iron oxide primary colloids. Analyzed in the same way as in Figure S1.

S3. Composite Nanoparticle Particle Size Distributions

Average particle sizes, as reported in Figure 3 of the main text, are a useful measure of the statistics of a nanoparticle distribution. However, it is valuable to also have the full particle size distributions (PSDs) which are reproduced here in Figures S6, S7, and S8 for each different sized iron oxide primary colloid species with three different molecular weights of co-core poly(styrene) at the four Flash NanoPrecipitation feed stream compositions. PSDs are all generally monodisperse (single log-normal distribution) and the magnetically captured fraction (open diamonds) aligns well with the initial, unseparated particle size distribution (solid circles). These size distributions also remain stable for at least 14 days. Some nanoparticles settle but shaking the dispersion by hand is sufficient to redisperse these sedimented nanoparticles. In these intensity-weighted size distributions, larger particles (with a larger scattering length density contrast against the surrounding aqueous dispersant due to the iron oxide content) will produce a larger signal which explains the agreement.

The non-magnetic fraction PSD (open triangles) is always smaller than the initial unseparated particles or the magnetically captured fraction. The small, 5.5 nm.d iron oxide primary colloids (Figure S6), produce nonmagnetic PSDs that show little overlap with the initial PSD while also producing very weak DLS scattering signals. The large, 28.7 nm.d iron oxide primary colloids (Figure S8) show considerable overlap between the nonmagnetic PSD while also producing strong DLS scattering signals. The average hydrodynamic diameters and distribution full width half maximum (FWHM) are tabulated for each formulation in Table S2. These DLS results are comparable to the TEM analysis of the different size iron oxide primaries. Small hydrophobic colloids are similarly sized to the hydrophobic polymer globules and diffuse similarly to both the hydrophobic homopolymer and stabilizer block copolymer which forms a

nearly homogeneous core phase of polymer, hydrophobic dye, and iron oxide primary colloids. Large hydrophobic colloids are similarly sized to large, nanoparticle-sized aggregates of hydrophobic polymers and diffuse much slower than the individual hydrophobic homopolymer and stabilizer block copolymer which forms heterogeneous populations of polymer-only “empty” nanoparticles and polymer aggregates containing iron oxide colloids. The medium sized primary iron oxide colloids (Figure S7) are an intermediate case, where some formulations produce homogeneous composite nanoparticles or heterogeneous, “empty” polymer-only nanoparticle populations. The data from Figures S6, S7, and S8 are compressed in Figure S9 for easy side-by-side comparison of the average hydrodynamic diameters between formulations.

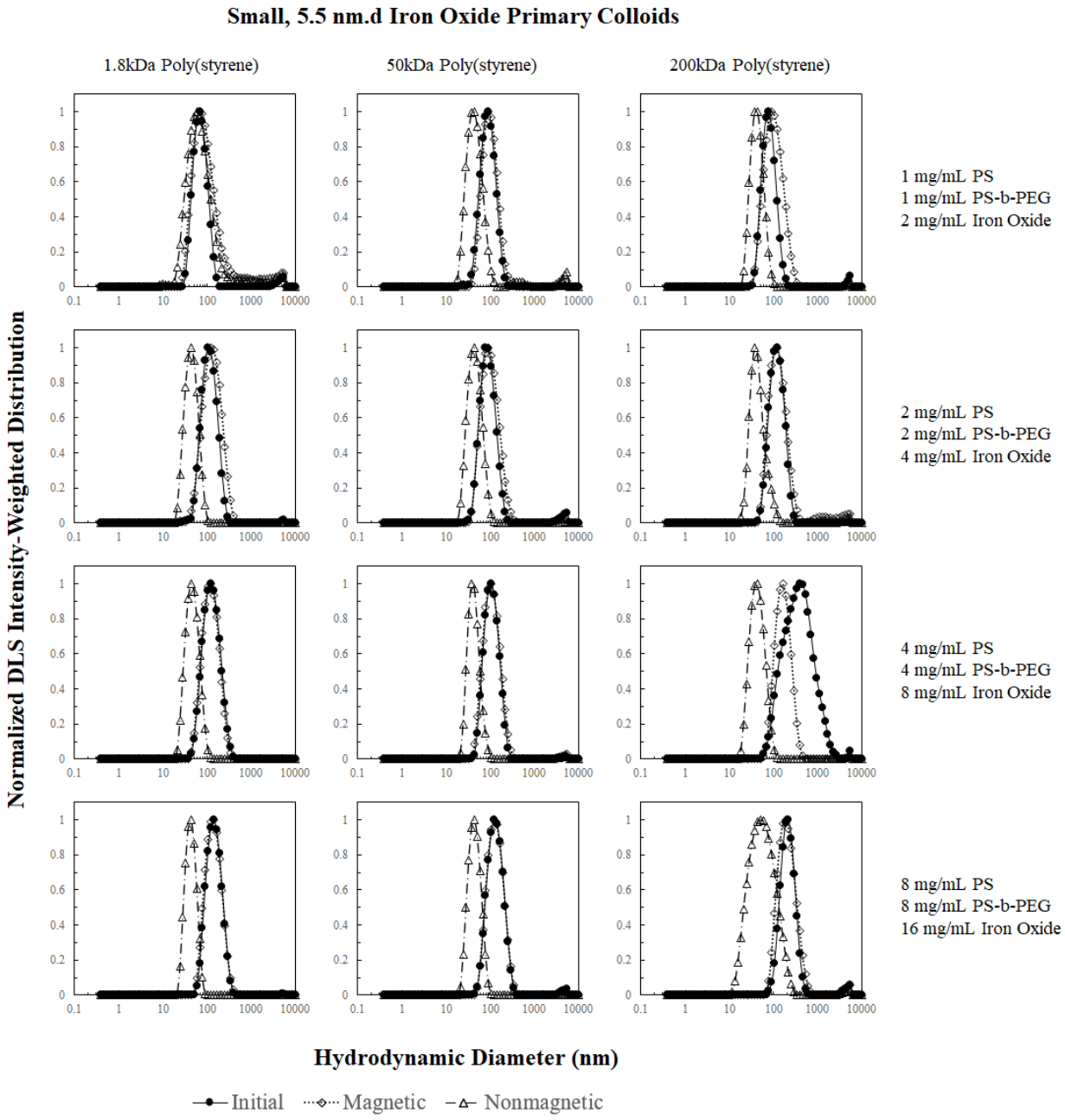

Figure S6. Particle size distributions of composite nanoparticles incorporating small (5.5 nm.d) iron oxide primary colloids.

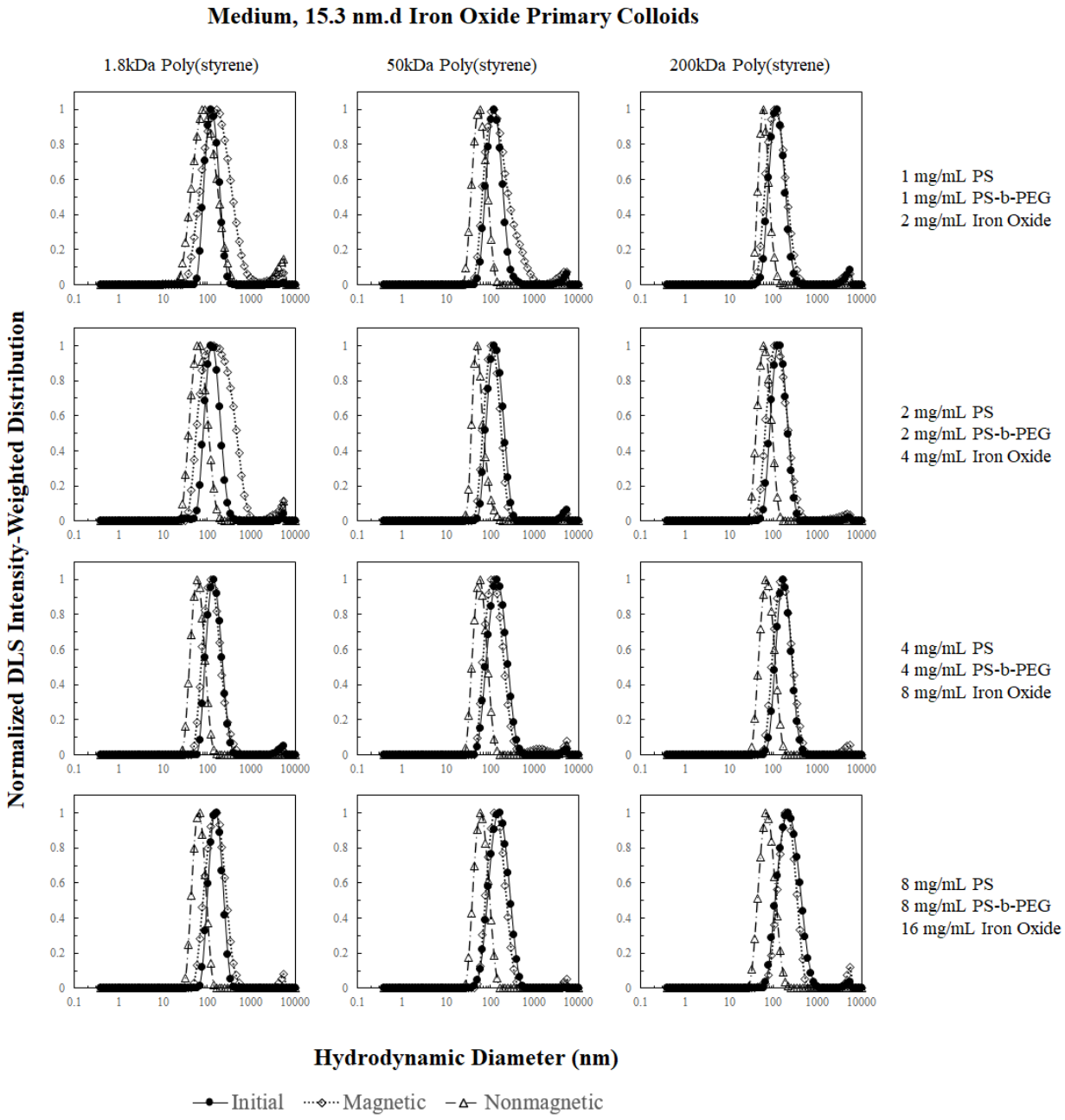

Figure S7. Particle size distributions of composite nanoparticles incorporating medium (15.3 nm.d) iron oxide primary colloids.

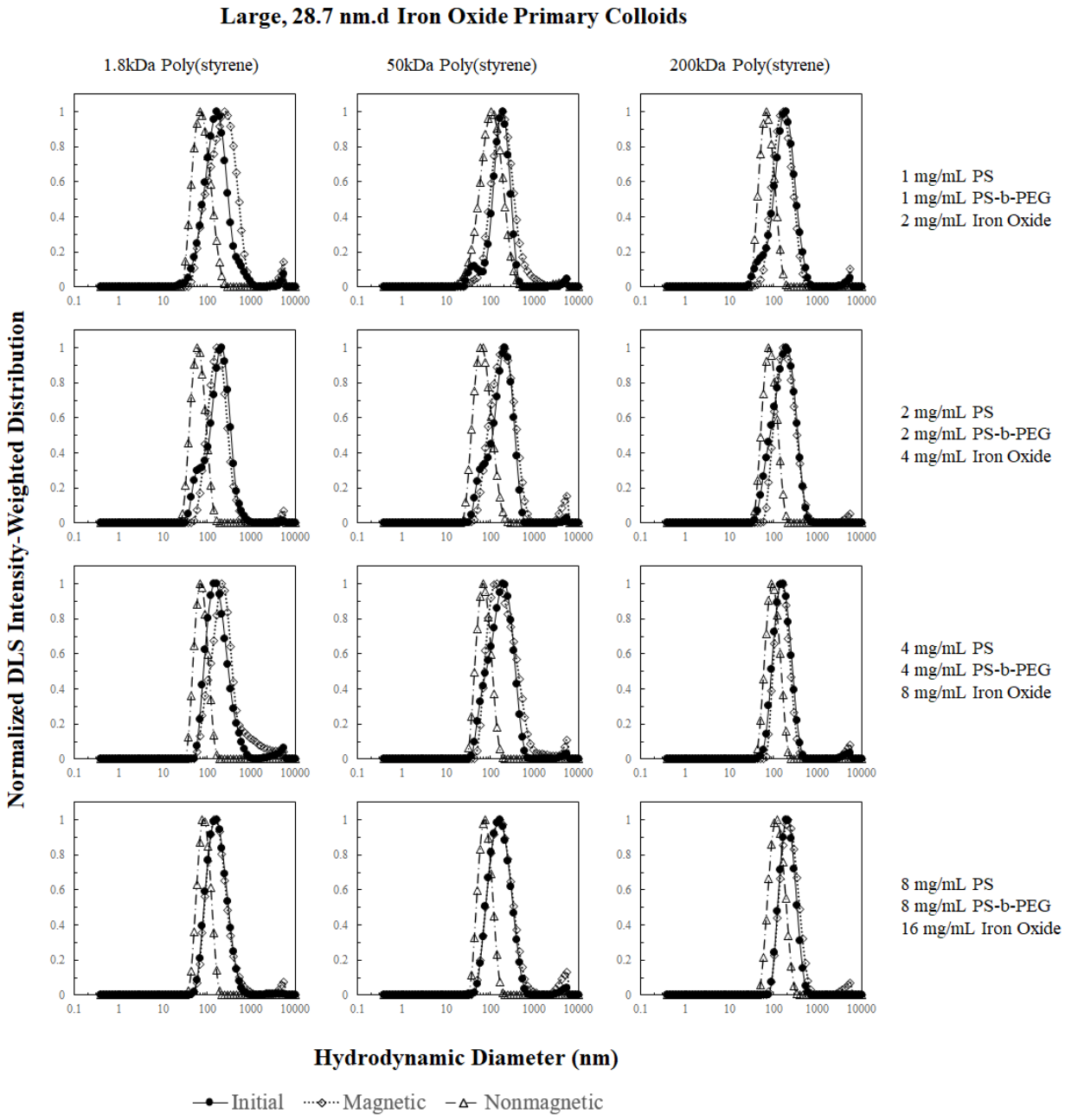

Figure S8. Particle size distributions of composite nanoparticles incorporating large (28.7 nm.d) iron oxide primary colloids.

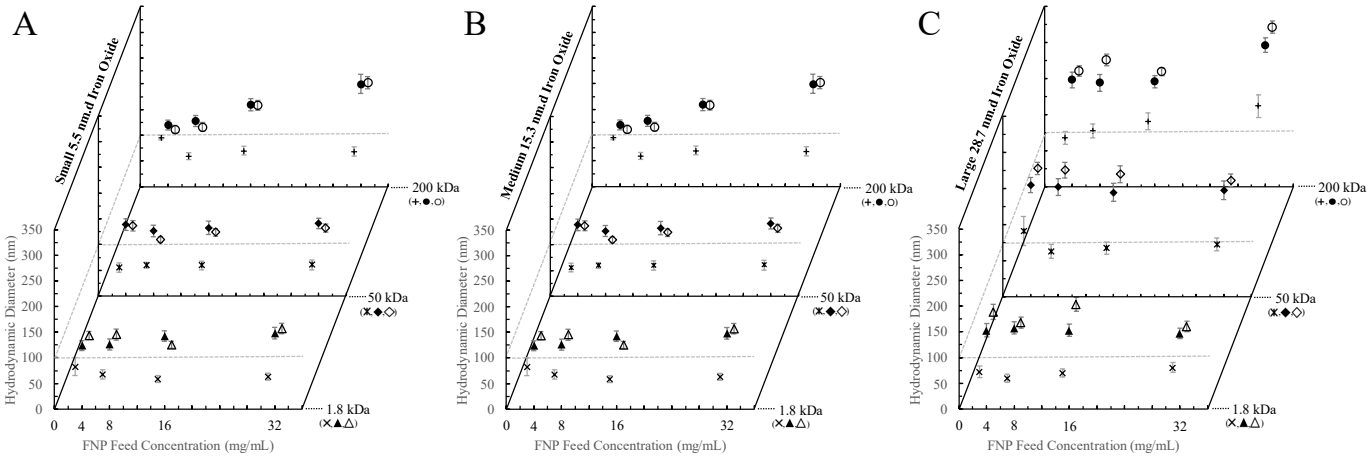

Figure S9. Intensity-weighted average hydrodynamic diameters of NPs prepared by Flash NanoPrecipitation loaded with magnetic iron oxide colloids. Error bars on each symbol are ± standard deviation of triplicate measurements of the formulation. From left to right, each group uses a different size of iron oxide primary colloid: A) small, B) medium and C) large. Inside of each group, from bottom to top, is a different PS co-core homopolymer MW: 1.8kDa, 50 kDa, and 200 kDa. Each individual plot combination of iron oxide primary colloid size and PS molecular weight contains three types of symbols: crossed line markers for the nonmagnetic fraction (×, ✶, and +), filled symbols for the initial dispersion containing magnetic and nonmagnetic NPs (▲, ◆, and ●), and open symbols for the magnetic fraction (△, ◇, and ○). The exact cross, filled, and open symbols vary between the PS molecular weights for clarity as indicated by the annotation by each axis. A dashed gray line is connected across all plots at the 100 nm diameter, to provide a reference datum in each PS MW series.

Table S2. Hydrodynamic Diameters Measured from Dynamic Light Scattering (1/3)

Iron Oxide Primary Colloid Size	Poly(styrene) Molecular Weight (kDa)	Feed Concentration (mg/mL)	Initial Dispersion		Nonmagnetic Fraction		Magnetic Fraction	
			Average Diameter ± STDEV (nm)	FWHM (nm)	Average Diameter ± STDEV (nm)	FWHM (nm)	Average Diameter ± STDEV (nm)	FWHM (nm)
Small, 5.5 nm diameter	1.8	4	69.0 ± 0.3	37.2	60.4 ± 0.7	46.2	83.2 ± 4.2	55.4
		8	104.1 ± 1.8	60.1	41.4 ± 0.5	40.7	115.6 ± 2.3	86.7
		16	114.0 ± 0.8	64.3	43.5 ± 0.8	43.7	110.8 ± 0.2	71.7
		32	126.7 ± 11.5	71.6	41.1 ± 0.2	35.9	129.2 ± 1.6	78.8
	50	4	83.5 ± 1.0	44.7	44.4 ± 1.0	46.3	97.1 ± 1.5	50.1
		8	84.4 ± 1.1	48.1	42.0 ± 0.4	43.6	91.4 ± 0.7	59.1
		16	100.5 ± 0.9	57.0	45.5 ± 4.4	30.7	101.8 ± 0.3	61.7
		32	123.0 ± 0.9	73.3	41.6 ± 0.6	38.4	121.5 ± 2.1	73.6
	200	4	78.9 ± 0.7	40.9	42.1 ± 0.9	37.4	91.7 ± 1.1	65.5
		8	109.8 ± 0.9	59.7	50.0 ± 9.3	33.8	122.4 ± 0.6	72.7
		16	185.2 ± 13.4	114.8	40.3 ± 1.1	44.4	153.7 ± 2.0	88.4
		32	215.5 ± 5.0	108.5	47.0 ± 1.6	28.2	193.0 ± 2.1	121.4

STDEV = standard deviation of the average hydrodynamic diameter across triplicate measurements of the NP formulation
FWHM = full width, half maximum of the distribution
Panel 1/3 of Table S2

Table S2. Hydrodynamic Diameters Measured from Dynamic Light Scattering (2/3)

Iron Oxide Primary Colloid Size	Poly(styrene) Molecular Weight (kDa)	Feed Concentration (mg/mL)	Initial Dispersion		Nonmagnetic Fraction		Magnetic Fraction	
			Average Diameter ± STDEV (nm)	FWHM (nm)	Average Diameter ± STDEV (nm)	FWHM (nm)	Average Diameter ± STDEV (nm)	FWHM (nm)
Medium, 15.3 nm diameter	1.8	4	123.9 ± 1.1	67.1	82.9 ± 2.9	79.5	144.0 ± 13.7	79.2
		8	126.0 ± 2.3	73.6	67.6 ± 6.7	71.8	145.2 ± 12.4	103.2
		16	142.4 ± 0.4	74.7	58.6 ± 0.8	53.8	125.1 ± 1.8	69.9
		32	147.8 ± 3.2	77.3	62.9 ± 1.0	55.8	157.1 ± 6.7	101.0
	50	4	139.0 ± 12.2	78.1	55.7 ± 1.3	53.8	136.8 ± 15.7	99.6
		8	126.6 ± 2.2	76.5	60.1 ± 5.0	33.8	109.5 ± 2.1	56.7
		16	132.3 ± 2.0	91.3	59.6 ± 1.1	51.6	123.8 ± 1.7	71.9
		32	141.2 ± 3.0	73.8	60.5 ± 1.2	59.1	131.6 ± 1.1	79.6
	200	4	119.8 ± 1.4	67.7	95.4 ± 15.2	39.4	111.8 ± 1.2	73.9
		8	128.0 ± 1.0	73.8	59.8 ± 1.6	55.7	116.4 ± 1.8	79.7
		16	159.4 ± 1.4	80.7	69.9 ± 1.7	68.0	158.5 ± 3.5	96.9
		32	199.8 ± 4.2	128.9	68.5 ± 1.3	72.3	202.2 ± 2.4	116.8

STDEV = standard deviation of the average hydrodynamic diameter across triplicate measurements of the NP formulation
FWHM = full width, half maximum of the distribution
Panel 2/3 of Table S2.

Table S2. Hydrodynamic Diameters Measured from Dynamic Light Scattering (3/3)

Iron Oxide Primary Colloid Size	Poly(styrene) Molecular Weight (kDa)	Feed Concentration (mg/mL)	Initial Dispersion		Nonmagnetic Fraction		Magnetic Fraction	
			Average Diameter ± STDEV (nm)	FWHM (nm)	Average Diameter ± STDEV (nm)	FWHM (nm)	Average Diameter ± STDEV (nm)	FWHM (nm)
Large, 28.7 nm diameter	1.8	4	153.1 ± 4.2	130.3	73.4 ± 2.0	90.4	189.1 ± 1.0	146.1
		8	157.7 ± 5.8	121.8	60.1 ± 2.6	61.7	168.2 ± 12.6	105.1
		16	152.9 ± 3.9	120.1	69.7 ± 2.1	64.6	204.3 ± 16.7	133.0
		32	146.9 ± 3.9	105.7	80.7 ± 1.9	76.1	160.7 ± 4.0	101.8
	50	4	155.0 ± 7.5	102.0	91.4 ± 1.7	79.5	178.2 ± 21.5	85.7
		8	152.3 ± 2.4	118.6	63.0 ± 3.3	78.8	175.7 ± 10.0	107.7
		16	144.9 ± 5.1	126.3	67.6 ± 1.2	68.9	170.0 ± 3.3	120.1
		32	147.5 ± 2.0	127.6	72.5 ± 2.1	70.7	161.2 ± 4.1	89.0
	200	4	148.0 ± 4.1	109.4	67.8 ± 1.6	71.5	160.5 ± 4.5	70.6
		8	143.9 ± 5.8	116.7	77.5 ± 2.8	78.8	175.6 ± 4.9	81.8
		16	145.6 ± 5.4	83.6	90.6 ± 3.2	91.0	159.3 ± 4.5	50.8
		32	196.0 ± 6.4	99.2	111.9 ± 4.6	126.1	221.2 ± 7.9	88.8

STDEV = standard deviation of the average hydrodynamic diameter across triplicate measurements of the NP formulation
FWHM = full width, half maximum of the distribution
Panel 3/3 of Table S2.

S4. TEM Images and Primary Colloid Aggregation Histograms

Representative TEM images for NPs combining medium or large primary colloids with the different PS molecular weights are shown in Figures S10 and S11. Individual histograms are shown below (Figures S12, S13, and S14) for the number of counted iron oxide primaries in each observed composite nanoparticle by TEM. For small primary colloids, no particles were reliably observed in the nonmagnetic fraction. For medium and large primary colloids, the distribution for both magnetic and nonmagnetic fractions are shown. This data is combined with the cross-sectional diameter of the nanoparticle to produce Figure 5 in the main text but is presented separately here for clarity. The individual symbols from Figure 5 are binned together (into pixels that are 5 nm wide and 5 counted primary colloids tall) into a heat map that shows the density of analyzed NPs in Figure S15. Nearly all combinations of polymer molecular weight and primary colloid size produce long "tails" in the distribution: low abundance nanoparticles with high aggregation numbers.

A Poisson distribution is also plotted on each histogram in Figures S10, S11, and S12 as a red line with circle markers. The usual Poisson probability mass function for k number of primary iron oxide colloids embedded in each nanoparticle is $f(k;\lambda) = \lambda^k e^{-\lambda}/k!$ where λ is determined as a fitting parameter by varying λ to minimize the sum of square error between the normalized observed data and the normalized Poisson distribution. Each distribution is normalized to a maximum value of 1. The Poisson fit shows good agreement with the observed data at low aggregation numbers, with a λ parameter like the median number of primary colloids per nanoparticle (the M value annotated in each panel), which suggests that these small NP cores assembly through the addition of monomers with similar average diffusion-aggregation time scales. TEM imaging of the composite nanoparticles also reveals a distribution tail composed of

nanoparticles with high primary colloid aggregation numbers that occur with low frequency. The Poisson distribution does not capture the existence of these larger nanoparticles due to the large value of *k* relative to the λ parameter, a fundamental limitation of the Poisson form. This suggests that the larger, high aggregation number nanoparticle cores form by collisions or mergers between smaller nanoparticle cores, which are described by the Poisson distribution as aggregates grown by diffusion-aggregation of individual primary colloids to the growing core. The newly merged cores yield a new single core with a large primary colloid aggregation number that occurs at extremely low probabilities in the indicated Poisson distribution.

Nonmagnetic nanoparticles show low Poisson parameters, $\lambda < 1$ with $\lambda \to 0$ for the nonmagnetic fraction prepared when using large iron oxide primary colloids. This is a consequence of the rare occurrence of primary colloids in the nonmagnetic fraction; for large iron oxide primary colloids, no iron oxide is observed in the nonmagnetic fraction. The sum of squares minimization yields $\lambda = 1 \times 10^{-6}$ for all the large primary colloid nonmagnetic fractions because no iron oxide primary colloids are observed in these nonmagnetic fractions, and the distribution of primary colloid aggregation number in this nonmagnetic population is a delta function at $k = 0$ which also collapses the corresponding Poisson distribution.

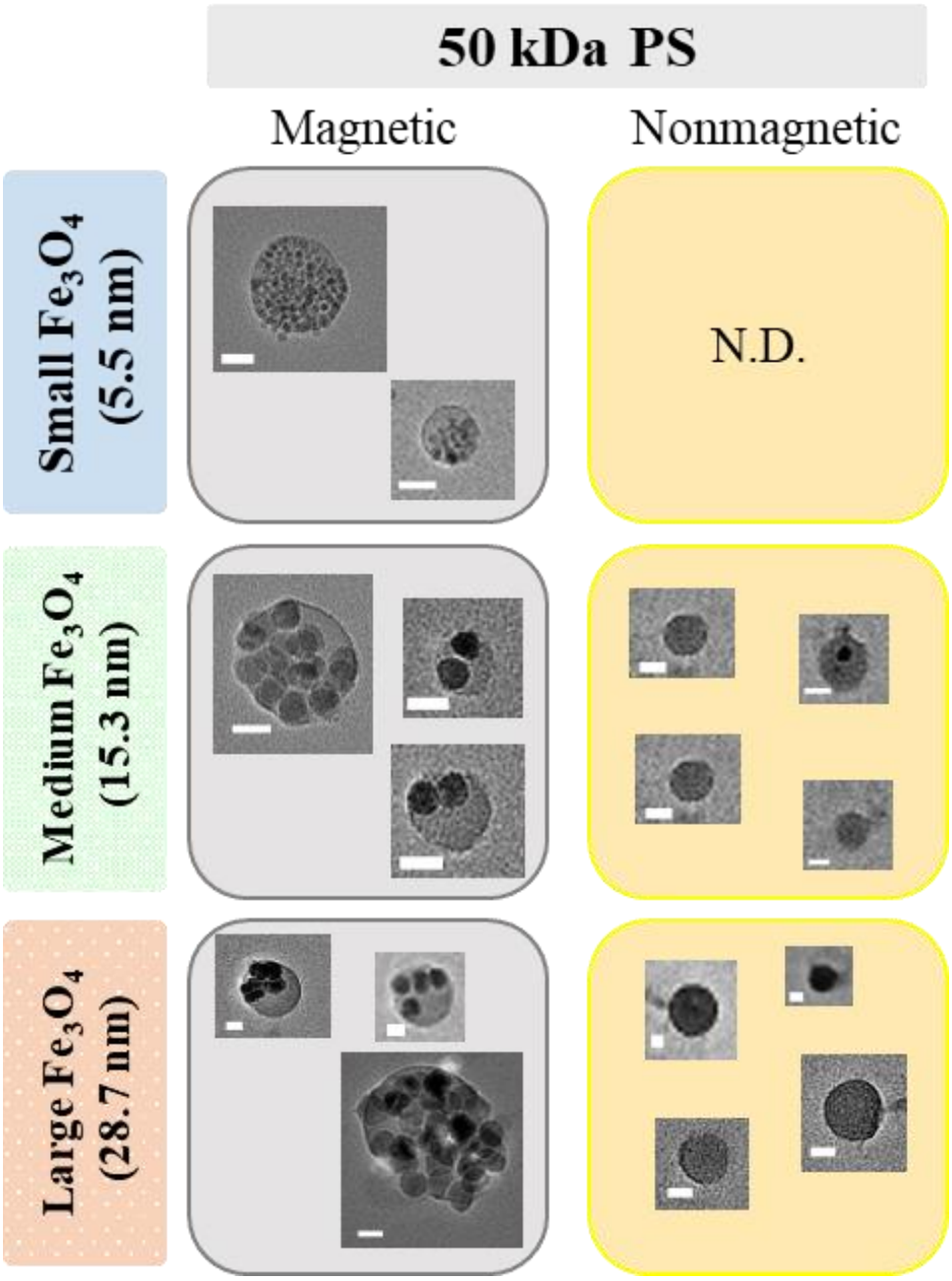

Figure S10. Representative TEM micrographs and particle microstructures for 50 kDa PS homopolymer. All micrographs contain a white scale bar of 20 nm. The nonmagnetic fraction of the small iron oxide primary colloids produced TEM grids without observable NPs as indicated by the not detected (N.D.) annotation.

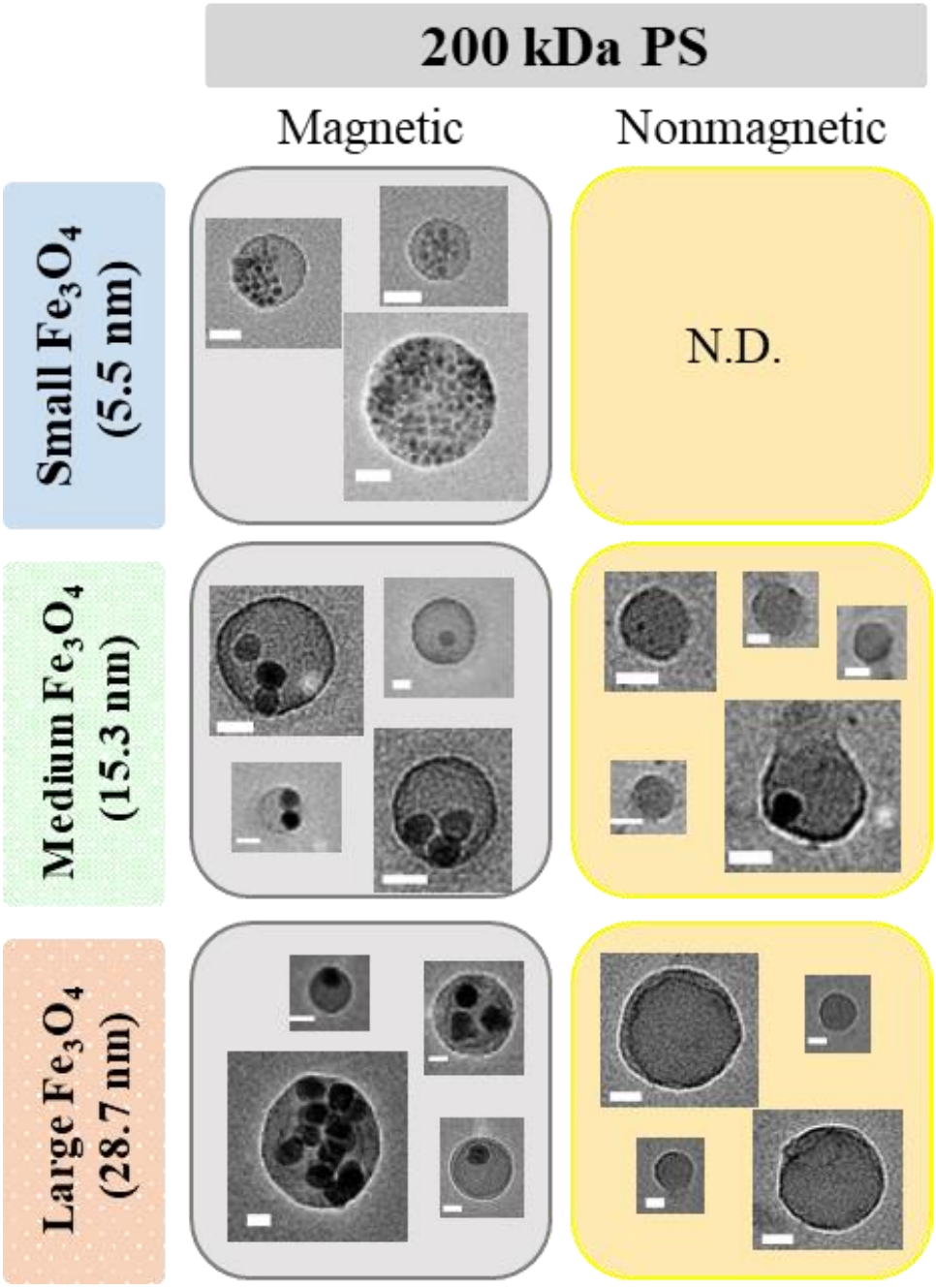

Figure S11. Representative TEM micrographs and particle microstructures for 200 kDa PS homopolymer. All micrographs contain a white scale bar of 20 nm. The nonmagnetic fraction of the small iron oxide primary colloids produced TEM grids without observable NPs as indicated by the not detected (N.D.) annotation.

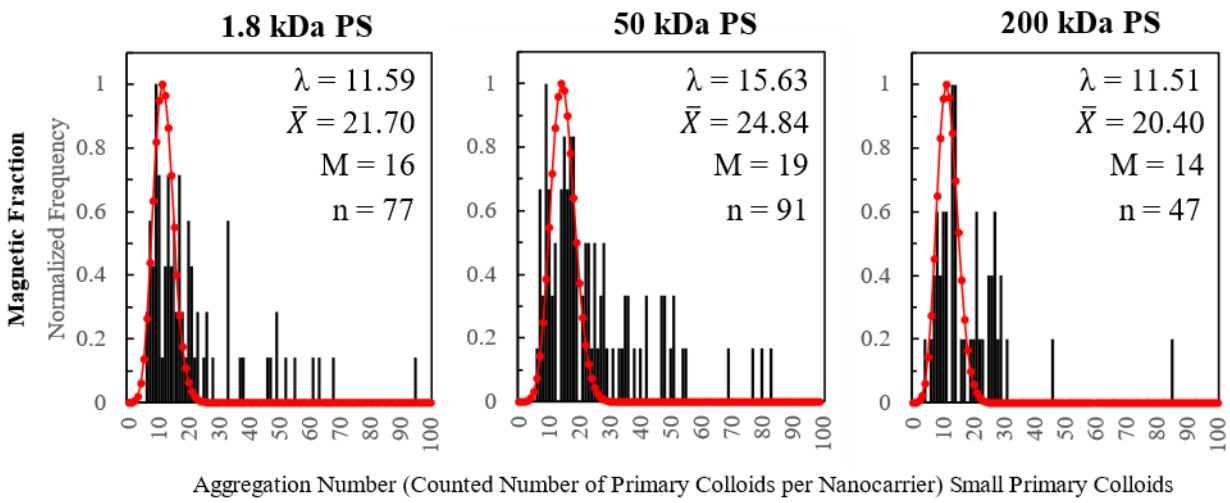

Figure S12. Small iron oxide primary colloids aggregation number histogram determined from TEM images. The number of iron oxide primary colloids in a nanoparticle is shown by the black barred X symbols connected with a dashed line to guide the eye. A Poisson distribution, using the λ value indicated in each panel, is also plotted as shown by the open red circles connected with a solid line. Each panel is annotated with the Poisson parameter, λ, the average number of primary colloids per nanoparticle, $\bar{X}$, the median number of primary colloids per nanoparticle, M, and the total number of observed nanoparticles, n. Only the magnetic fraction was observed with the small primary colloids, no nonmagnetic particles were imaged.

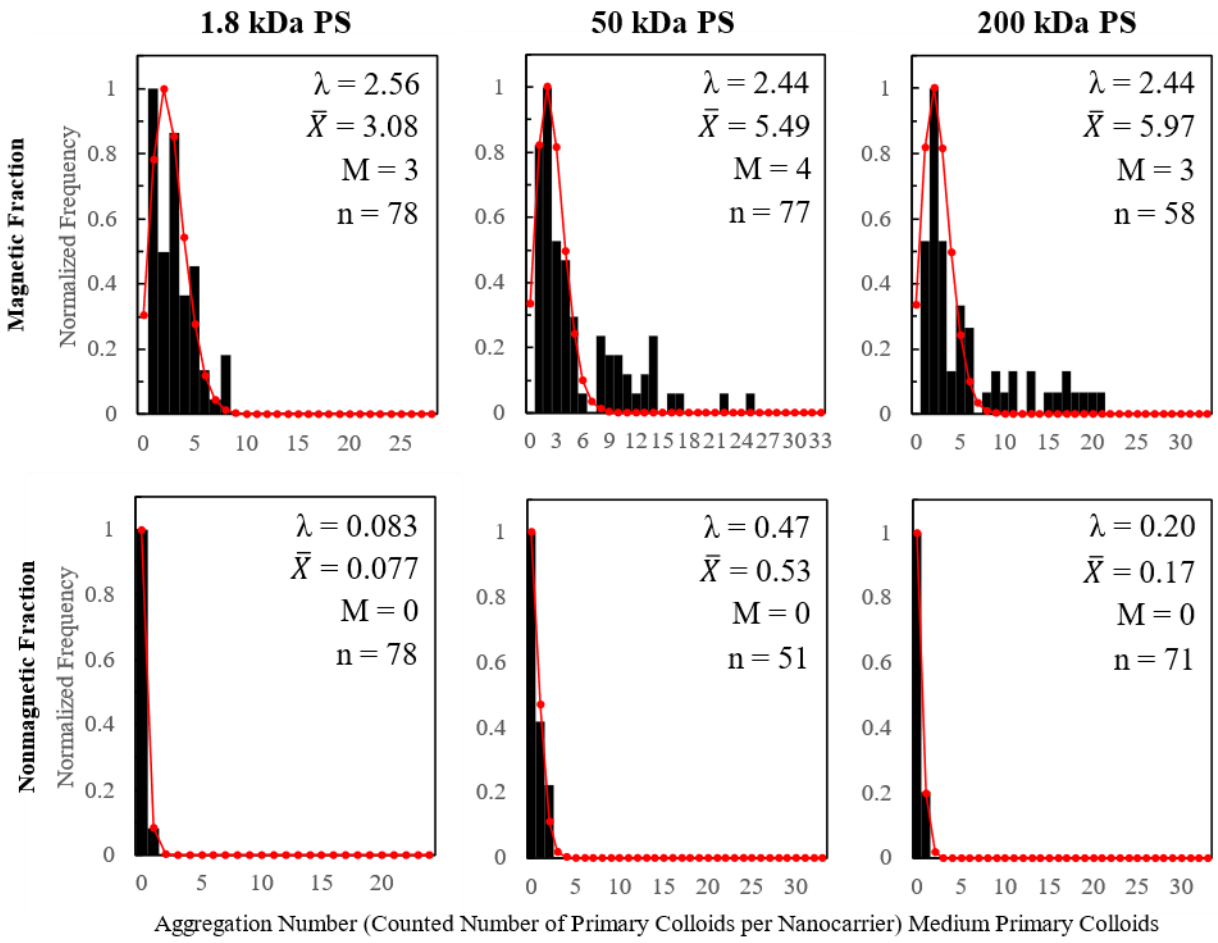

Figure S13. Medium iron oxide primary colloids aggregation number histogram. The number of iron oxide primary colloids in a nanoparticle is shown by the black barred X symbols connected with a dashed line to guide the eye. A Poisson distribution, using the λ value indicated in each panel, is also plotted as shown by the open red circles connected with a solid line. Each panel is annotated with the Poisson parameter, λ, the average number of primary colloids per nanoparticle, $\bar{X}$, the median number of primary colloids per nanoparticle, M, and the total number of observed nanoparticles, n. Both the magnetic (top row) and nonmagnetic (bottom row) populations are shown.

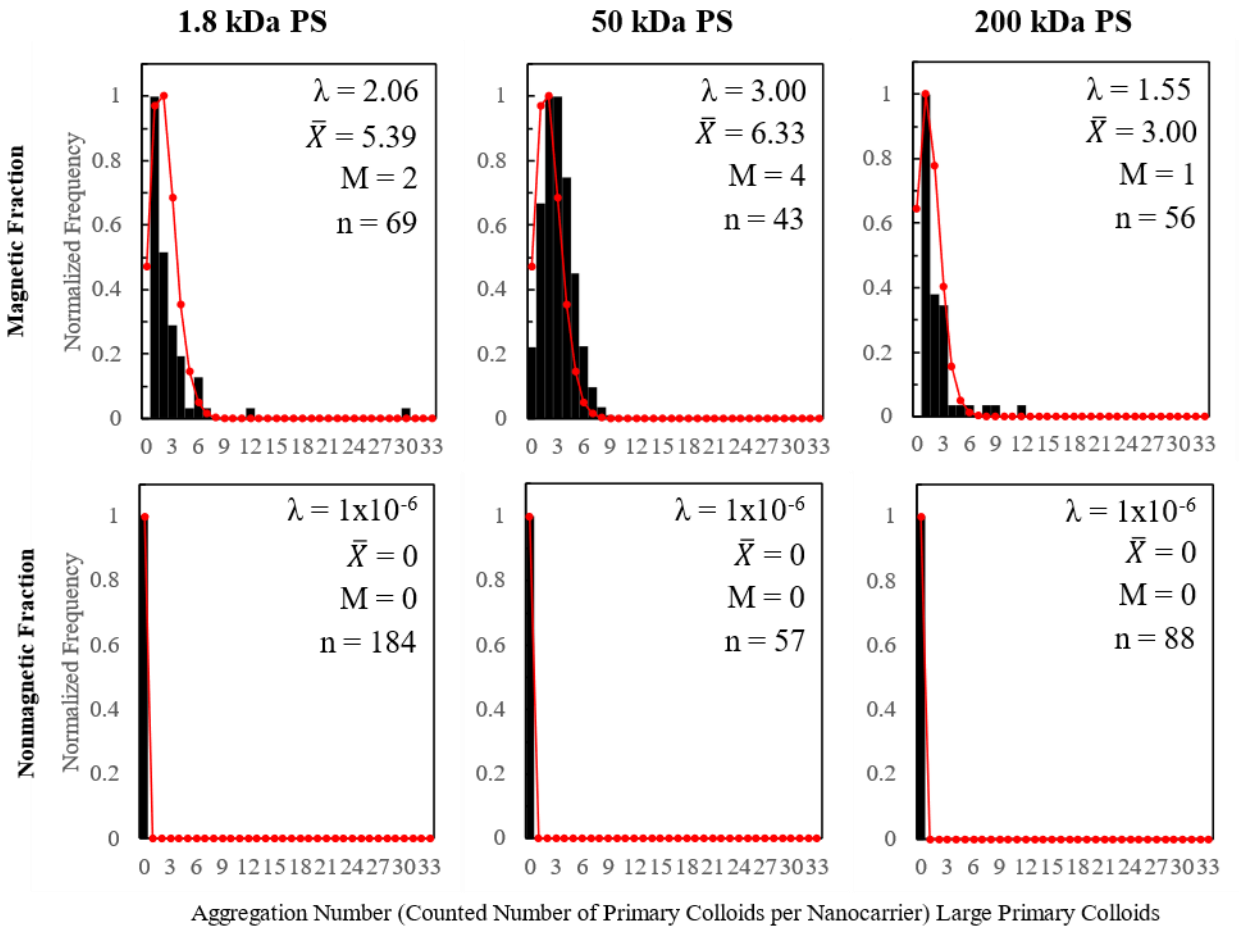

Figure S14. Large iron oxide primary colloids aggregation number histogram. The number of iron oxide primary colloids in a nanoparticle is shown by the black barred X symbols connected with a dashed line to guide the eye. A Poisson distribution, using the λ value indicated in each panel, is also plotted as shown by the open red circles connected with a solid line. Each panel is annotated with the Poisson parameter, λ, the average number of primary colloids per nanoparticle, $\bar{X}$, the median number of primary colloids per nanoparticle, M, and the total number of observed nanoparticles, n. Both the magnetic (top row) and nonmagnetic (bottom row) populations are shown.

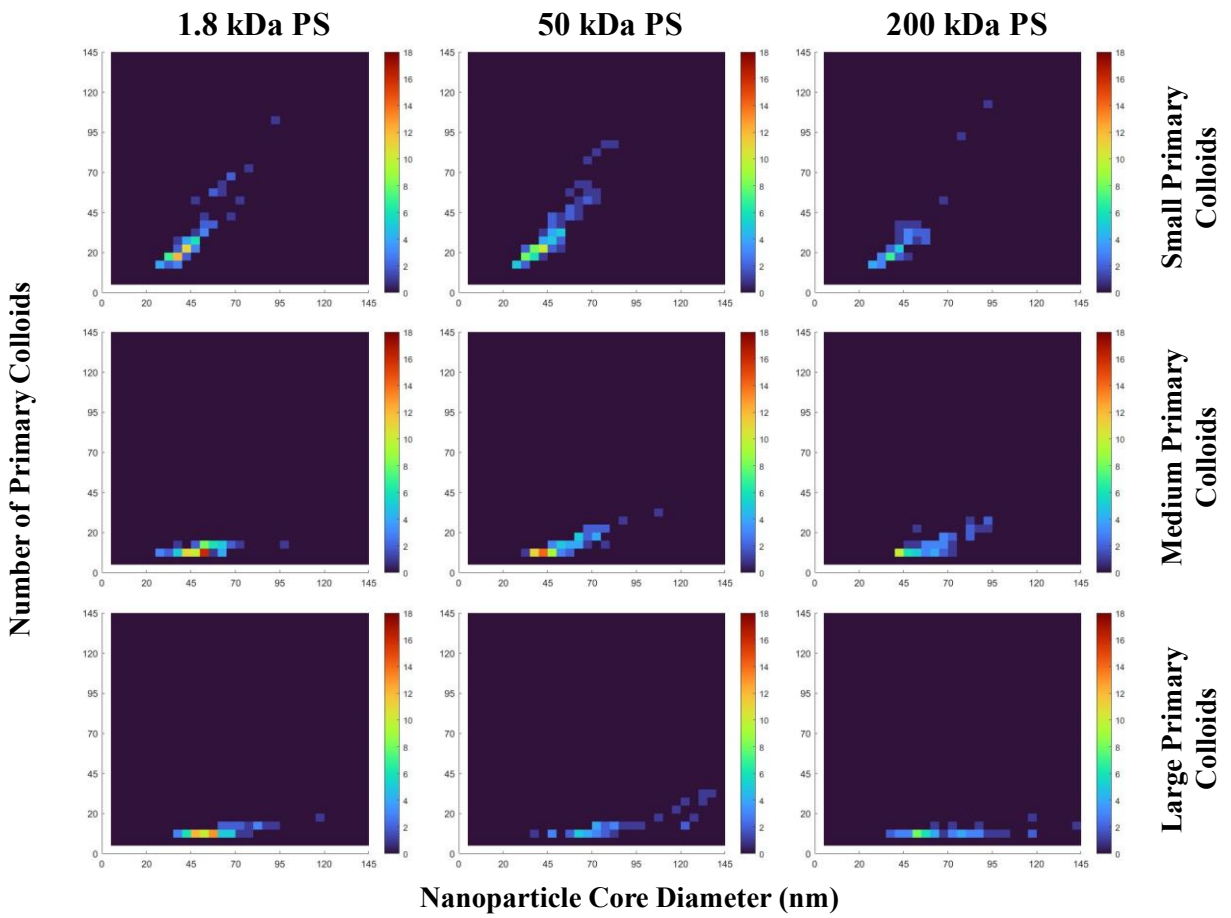

Figure S15. Density map of observed composite NP points from Figure 6. Each pixel is a 5x5 bin, representing a bin width of either 5 counted primary colloids or 5 nanometers on the measured NP core diameter.

Table S3. Effective Hydrodynamic Radii of Nanoparticle Components

	1.8kDa PS	50kDa PS	200kDa PS	"Small" Iron Oxide	"Medium" Iron Oxide	"Large" Iron Oxide	PS-b-PEG
Effective Radius (nm)	0.88	2.66	4.23	2.75	7.65	14.35	3.52

S5. Diffusion Time Scale Model

The Flash NanoPrecipitation (FNP) process is a micromixing technique that exploits a rapid change in solvent quality to induce supersaturation of material that promotes conditions for homogeneous nucleation and growth. Growth is arrested at typical nanoparticle sizes (40-200 nm.d) by a stabilizer. This high-level view explains the monodisperse, monomodal particles produced from FNP. A microscopic view of FNP is also helpful to gain insights into the particle assembly process that is fundamentally a diffusion-limited aggregation (DLA) of hydrophobic core materials which are stabilized by slower-adsorbing reaction-limited aggregation (RLA) block copolymers. Johnson, in the original literature on FNP, succinctly describes this as a case of requiring matched time scales to produce protected nanoparticles: particle core assembly must happen before or contemporaneous with stabilizer adsorption.[1,2] Mismatched process time scales can lead to the production of macroscopically aggregated core material (insufficient stabilizer adsorption to arrest growth at nanoscale) and "empty" stabilizer micelles that contain no core materials.

All iron oxide primary colloids synthesized here are organic-dispersible due to the dense surface coating of adsorbed oleate ions but differ substantially in size. Small, medium, and large species cover almost a full order of magnitude (from 5.5 nm.d to 28.7 nm.d) change in the particle diameter. Similarly, using different poly(styrene) molecular weights changes the hydrodynamic size of both solvated polymer coils and collapsed, hydrophobic polymer globules.

A hydrophobic homopolymer in dilute solution, such as PS in THF, will collapse to form globules where each globule consists of only one polymer chain. These globules then diffuse and aggregate to form a nanoparticle core before being stabilized by adsorbed block copolymer. The equation describing the radius, R_{PS}, of a theoretically dense collapsed PS globule is given in Equation S3 below, where MW is molecular weight in Daltons (g/mole), N_A is Avogadro's number, and ρ is the bulk density of poly(styrene). Molecular weight has a weak effect ($MW^{1/3}$) effect on globule size but large changes in MW, which can be realized with polymers such as PS, can produce significant globule sizes. For 1.8kDa PS, the globule radius is 0.88 nm; for 50kDa PS, the globule radius is 2.66 nm; and for 200kDa PS, the globule radius is 4.23 nm.

$$R_{PS} = \left(\frac{MW_{PS}\,[Da]}{\frac{4}{3}\pi\, N_A\, \rho \left[\frac{g}{mL}\right] * 10^{-21}} \right)^{1/3} = \left(\frac{MW_{PS}[Da]}{\frac{4}{3}\pi\, N_A\, \rho \left[\frac{g}{nm^3}\right]} \right)^{1/3} [=]\, nm \qquad \text{(Eqn S3)}$$

All formulations use the same poly(styrene)-b-poly(ethylene glycol) (PS-b-PEG) stabilizer: a 1.6kDa PS block and a 5.0kDa PEG block. The molecular dimensions of this molecule cannot be calculated as easily as the polystyrene because the PEG block remains solvated during FNP and occupies a much larger volume than a collapse polymer globule. Instead, the block copolymer size is estimated from the sum of the effective, hydrodynamic PEG coil radius and the collapsed PS globule radius, as given in Equation S4 below, where $[\eta]$ is the intrinsic viscosity of PEG in tetrahydrofuran, calculated from published Mark-Houwink-Sakurada parameters as usual ($[\eta] = K * MW^a$). The characteristic dimensions of all PS, PS-b-PEG, and iron oxide species during nanoparticle assembly is given in Table S3.

$$R_{BCP} = R_{PS}(1.6kDa) + \left(\frac{MW_{PEG}\,[\eta]\left[\frac{mL}{g}\right] * 10^{21}}{\frac{4}{3}\pi\, N_A} \right)^{1/3} \qquad \text{(Eqn S4)}$$

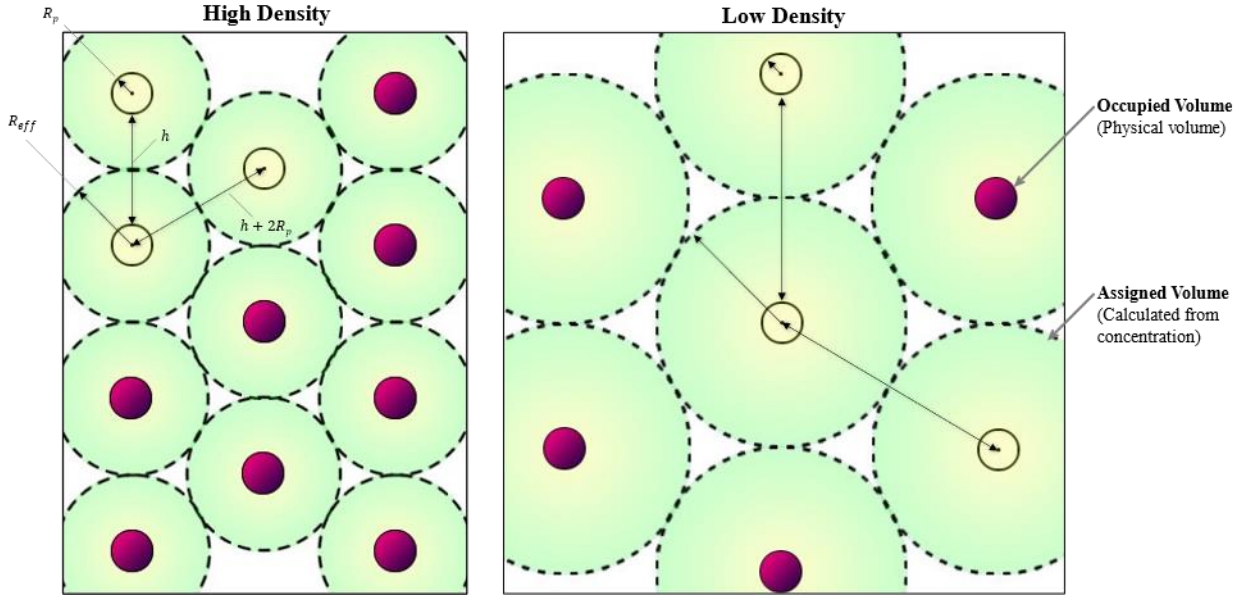

Figure S16. Graphical representation of average distances between generic particles of radius R_p in dispersion. The image represents a 2D slice of a dispersion where particle locations are represented by a central sphere (filled or empty). These locations have been constrained to hexagonal lattice locations to demonstrate the surface-to-surface distance calculation. Surface-to-surface distance, h, is determined by calculating an effective volume that each particle occupies before encountering an adjacent particle. Because the effective volume assigned to each individual particle is a sphere of radius R_{eff}, the total volume of the dispersion, V_{total}, is not fully accounted for, as evident with the white areas between effective volume spheres. The accounted-for volume is $\phi_{max}V_{total}$ where ϕ_{max} is the maximum volume packing fraction of homogeneous spheres, 0.64 for uniform sphere close-packing. When the particle concentration (volume fraction) changes, the particle radius, R_p, remains unchanged but the interparticle spacing, h, changes.

Single-Component Systems: Distance Between Surfaces & Time Scale of Diffusion

Different sized particles, at the same mass concentrations, have different number densities. For example, poly(styrene) at 1 mg/mL would have number densities of $3.34*10^{17}$ polymers/mL (1.8kDa), $1.20*10^{16}$ polymers/mL (50 kDa), and $3.01*10^{15}$ polymers/mL (200kDa). This makes evident that the different sized homopolymer globules have different surface-to-surface distances. The center-to-center distance can be easily calculated but we are primarily concerned with the surface-to-surface distance as hydrophobic homopolymers form nanoparticles through diffusion-limited aggregation where only surface contacts are required to form an aggregate of two polymer globules; considering each globule as a hard sphere (over short times polymers will not relax and form entanglements between globules) also means that globule centers can never intersect, only globule surfaces.

Determining the surface-to-surface distance between particles in a dispersion requires a simple geometric consideration of how the particles of a dispersion fill space, both in the physically occupied space of the dense, hard core of the particle and how much volume is in between each particle. The total volume of a dispersion can be normalized by the number of particles in dispersion, giving an effective volume, V_{eff}, as below in Eqn. S5, that each particle may wander within before encountering the volume of an adjacent particle. This volume, and the associated radius is depicted graphically in Figure S16. In Eqn S5, V_{max} is the maximum volume that close-packed sphere could occupy in the total dispersion volume, which is equivalent to the physical total volume, V_{total}, multiplied by the maximum volume fraction, ϕ_{max}. V_{eff} is treated as close-packed spheres because the volume will be converted into a radius that defines the boundary surface between adjacent particles and the packing of these hypothetical spheres requires compensating for the maximum volume fraction of said spheres (some of the total

physical volume is neglected without this correction). N_p is the number of particles, which is equal to the concentration of particles, C_p, multiplied by the total volume, V_{total}, divided by the specific mass of each particle, $\overline{m_p}$, as defined in Eqn S6. Combining Equations S5 and S6 yields Eqn S7.

$$V_{eff} = \frac{V_{max}}{N_p} = \frac{V_{max}}{C_p V_{total}/\overline{m_p}} = \frac{V_{Total} * \phi_{max}}{C_p * V_{total}/\overline{m_p}} = \frac{\phi_{max}\overline{m_p}}{C_p} \quad \text{(Eqn S5)}$$

$$\overline{m_p} = \frac{4}{3}\pi R_p^3 * \rho_p \quad \text{(Eqn S6)}$$

$$R_{eff} = \left(\frac{V_{eff}}{\frac{4}{3}\pi}\right)^{1/3} = \left(\frac{\phi_{max} * \frac{4}{3}\pi R_p^3 * \rho_p}{\frac{4}{3}\pi C_p}\right)^{1/3} = R_p\left(\frac{\phi_{max} * \rho_p}{C_p}\right)^{1/3} \quad \text{(Eqn S7)}$$

Equation S7 can be further simplified by defining the volume fraction of particles, as in Eqn S8 below. The colloidal species density is used as this yields the correct value of $\phi \to 1$ and $C_p \to \rho_p$ when $\rho_p > \rho_{solvent}$ is typical. At usual FNP concentrations, $C_p/\rho_p \approx C_p/\rho_{solvent}$ due to the use of comparatively dilute solutions. This yields Eqn S9, which gives the effective radius of the "effective volume sphere" assigned to each particle as a function of the intrinsic, hard-core particle radius and the concentration (volume fraction) of particles in dispersion. This can the be readily converted into the surface-to-surface separation distance, h, as in Eqn S10. This distance represents and average or thermal equilibrium distance between particles; concentration fluctuations and movement of independent colloids will mean some local surface-to-surface distances are larger or smaller than the value calculated here.

$$\frac{C_p}{\rho_p} \approx \phi \qquad \text{(Eqn S8)}$$

$$R_{eff} = R_p \left(\frac{\phi_{max}}{\phi}\right)^{1/3} \qquad \text{(Eqn S9)}$$

$$h = 2R_{eff} - 2R_p = 2\left[R_p \left(\frac{\phi_{max}}{\phi}\right)^{1/3}\right] - 2R_p = 2R_p \left[\left(\frac{\phi_{max}}{\phi}\right)^{1/3} - 1\right] \qquad \text{(Eqn S10)}$$

Diffusion Time Scale for Particles

The surface-to-surface spacing provides a characteristic length scale for particles to traverse before aggregation and growth occurs during particle assembly. This length scale can be converted to a time scale (average time between particle collisions/aggregation events at the start of Flash NanoPrecipitation) through the diffusion coefficient and its usual dimensions of length squared per time. Calculating this rate or lag time for each species is of interest because of the phenomenon seen with the medium and large iron oxide primary colloids where "empty" nanoparticles with only polymer cores are produced. Increasing the molecular weight of the hydrophobic core poly(styrene) decreases the fraction of material lost in these "empty" nanoparticles. We believe this is reflected by slower diffusion of the large, colloidal species of iron oxide primary colloids. Low molecular weight homopolymer and block copolymer can diffuse, aggregate, and stabilize isolated particles before adjacent iron oxides diffuse and aggregate with the growing particle core. For medium-sized iron oxides (15.3 nm.d) increasing the polymer molecular weight to 50 kDa or 200 kDa mostly eliminates these "empty"

nanoparticles while large-sized iron oxides always produce significant “empty” nanoparticles (see the composition measurements in Figure 4 of the main text, the %HY3G captured reflects how much dye-stained hydrophobic material is magnetically captured.) Even the 200kDa PS globule is smaller than the medium-sized iron oxide primary colloids, so core species do not have to be identically sized but must be “close enough” within some criterion.

We establish the criterion for how “similarly sized” or “close enough” different hydrophobic materials must be to form homogeneous nanoparticles based on a time scale for each hydrophobic species to diffuse and aggregate across the characteristic interparticle spacing. In this model, each component is considered in isolation; distances are for poly(styrene) to poly(styrene) globule aggregation or iron oxide to iron oxide aggregation where the characteristic time depends on the size and concentration of the aggregating species. This component-wise consideration enables a simple model where each component has a straightforward, explicit expression for a characteristic initial aggregation time scale, analogous to a Smoluchowski time constant.

The diffusion coefficient, $\mathcal{D}$, is given by Stokes-Einstein for a spherical particle as written in Eqn S11. This provides both a diffusivity and coupling of length and time scales via the dimensionality of the diffusivity in length squared per time, L^2/t. A characteristic time, τ_i, can be calculated from the diffusivity and the surface-to-surface spacing as in Eqn S12 below. Eqn S13 shows the proportionality between the characteristic time and the particulate concentration (as volume fraction) by expansion of the squared term in Eqn S12; the characteristic time τ_i scales with the term $[(\varphi_{max}/\varphi_i)^{1/3}\text{-}1]^2$ neglecting the proportionality constant $24\pi\eta R_i^3/k_BT$. The squared volume fraction term causes the characteristic time to scale primarily by $(1/\phi)^{2/3}$ at low

concentrations but deviates at higher concentrations due to the $(1/\phi)^{1/3}$ term (Eqn S13), which explains the lines of constant time in Figure 8 on a log-log plot.

$$\mathcal{D} = \frac{k_B T}{6\pi\eta R_p} \quad \text{(Eqn S11)}$$

$$\tau_i = \frac{h^2}{\mathcal{D}} = \frac{6\pi\eta R_i}{k_B T}\left\{2R_i\left[\left(\frac{\phi_{max}}{\phi_i}\right)^{1/3} - 1\right]\right\}^2 = \frac{24\pi\eta R_i^3}{k_B T}\left[\left(\frac{\phi_{max}}{\phi_i}\right)^{1/3} - 1\right]^2 \quad \text{(Eqn S12)}$$

$$\tau_i \propto \left(\frac{\phi_{max}}{\phi_i}\right)^{2/3} - 2\left(\frac{\phi_{max}}{\phi_i}\right)^{1/3} - 1 \quad \text{(Eqn S13)}$$

The constant, physical parameter prefactor, $24\pi\eta/k_B T$, cancels when considering the ratio of the characteristic time scales for the iron oxide (*i* component) and the poly(styrene) (*j* component). This relationship is the basis of the ratio metric plotted in Figure 9 of the main text, where the critical value of $\tau_i/\tau_j \leq 30$ is established by comparing against the capture efficiency of the Hostasol Yellow 3G dye in each formulation. These ratios are tabulated in Table S4 for the different poly(styrene) and iron oxide primary colloid combinations.

$$\frac{\tau_i}{\tau_j} = \frac{R_i^3\left[\left(\frac{\phi_{max}}{\phi_i}\right)^{1/3} - 1\right]^2}{R_j^3\left[\left(\frac{\phi_{max}}{\phi_j}\right)^{1/3} - 1\right]^2} \quad \text{(Eqn S14)}$$

Multicomponent Systems: Occupied Volume

Flash NanoPrecipitation takes a feed stream containing several different species that combine to form the desired nanoparticles. Indeed, we make use of polymers and inorganic iron oxides in this study to make composite, magnetically-responsive nanoparticles. Previously the model put forth considered one component at a time. This was motivated by seeking to develop a simple model that accounts for both the diffusivity of a colloidal species and the distance it must diffuse to aggregate with other colloids of the same species.

In multicomponent FNP the distance between particles or colloidal species requires the consideration of every component. As before, the distance between species can be determined by extending the radius of each species, R_i, to an effective radius. However, the different intrinsic R_i of each species means R_{eff} will be different for each species. This can be reduced to a set of similar variables by defining $R_{eff,i} = R_i + R^*$, where R^* is the "radius increase" of each single species to project an effective volume assigned to each particle sphere. This is depicted graphically in Figure S17, a modified annotated version of Figure 7 in the main text. This inter-particle spacing for multiple components is given by Equation S15 with the derivation below.

$$\phi_{max} = \sum \phi_i \frac{(R_i + R^*)^3}{R_i^3} \qquad \text{(Eqn S15)}$$

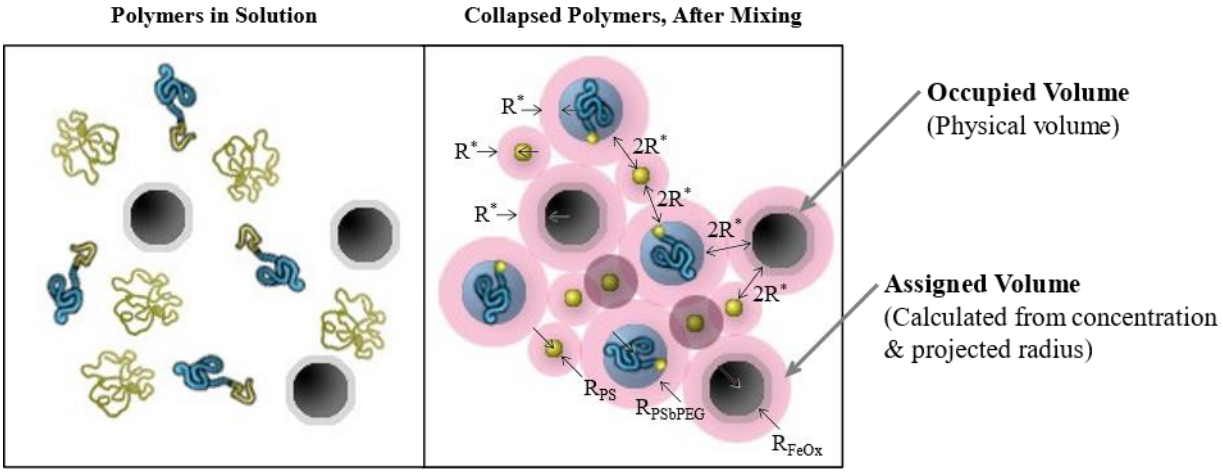

Figure S17. Spacing between multiple components during FNP assembly. The diagram is considered more a cartoon than Figure S16, which explicitly implemented hexagonal spacing, for exact positioning of the component species. PS: yellow ribbons and collapsed sphere, PEG: blue ribbons, iron oxide: black spheres. PS-b-PEG is surrounded by a blue sphere to represent the hydrodynamic size of the solvated PEG block. The surface of each species is extended by an amount R^* to create a different effective radius, $R_{eff,i} = R_i + R^*$, for each species. The common R^* means each species has the same thickness of assigned volume shell, where the total volume changes based on the core radius, R_i, of each species.

Consider a system with a total volume, V_{total}, as before, and ϕ_{max}, the maximum packing fraction of spheres used to divide this volume up. The total available volume is $V_{total}\phi_{max}$ as before. Now the volume assigned to any one species is the sum of the occupied volume, intrinsic to each particle based on its intrinsic physical radius R_i, plus the volume of the spherical shell of "assigned" volume with a thickness of R^*, for total spherical volume of $\frac{4}{3}\pi(R_i + R^*)^3$, multiplied by the number of particles present, N_i. Summation over the volume assigned to each particle equals the total available volume.

$$V_{total}\phi_{max} = \sum N_i * \frac{4}{3}\pi(R_i + R^*)^3 \qquad \text{(Eqn S16)}$$

The number density is calculated in the same way as Eqns S5 and S6 above, explicitly restated in Eqn S17 below. Substituting this expression for N_i, and using Eqn S8, $C_i \backslash \rho_i \approx \phi_i$, an implicit equation is found.

$$N_i = \frac{C_i V_{total}}{\overline{m_i}} = \frac{C_i V_{total}}{\frac{4}{3}\pi R_i^3 * \rho_i} \qquad \text{(Eqn S17)}$$

$$V_{total}\phi_{max} = \sum \frac{C_i V_{total}}{\frac{4}{3}\pi R_i^3 * \rho_i} * \frac{4}{3}\pi (R_i + R^*)^3 = V_{total} \sum \phi_i \frac{(R_i + R^*)^3}{R_i^3} \qquad \text{(Eqn S18)}$$

Cancelling the V_{total} found on both sides renders the result insensitive to the total volume, as expected. Again, the expression is an implicit function for R^*, where $h = 2R^*$, in Eqn S19. This is identical to the presented form in Eqn S15 above. This model produces one surface-to-surface distance, which reduces the ratio of characteristic time scales (Eqn S14) to simply the ratio of colloid diffusivities or $\tau_i/\tau_j = R_j/R_i$. This implementation buries some of the nuance that different sized colloidal entities have different specific masses and number densities that contribute to changing interparticle spacing that alters the characteristic time scale for each species. Our analysis uses the simple, one-component-at-a-time model of Eqns S12 and S14 as it is an explicit, easily calculated function for any generic combination of species. This mutual model of Eqn S19 is more useful for detailed considerations of the assembly process but provides only an implicit function for multiple components.

$$\phi_{max} = \sum \phi_i \frac{(R_i + R^*)^3}{R_i^3} \qquad \text{(Eqn S19)}$$

Reducing Eqn S19 to a single component recreates the previously derived surface-to-surface spacing in Eqn S10.

$$\phi_{max} = \phi \frac{(R_i + R^*)^3}{R_i^3}, or\ R^* = R_i \left[\left(\frac{\phi_{max}}{\phi} \right)^{\frac{1}{3}} - 1 \right] \quad \text{(Eqn S20)}$$

Table S4. Ratio of Iron Oxide to Poly(styrene) Characteristic Time Scales

Component Concentrations				τ_{FeOx}/τ_{PS}		
Iron Oxide Primary	[PS-b-PEG] (mg/mL)	[PS] (mg/mL)	[Fe3O4/OA] (mg/mL)	1.8k PS (0.88 nm)	50k PS (2.66 nm)	200k PS (4.23 nm)
Small (2.75 nm)	1	1	2	24.6	0.886	0.221
	2	2	4	24.6	0.881	0.220
	4	4	8	24.3	0.874	0.218
	8	8	16	24.0	0.865	0.216
Medium (7.65 nm)	1	1	2	632	22.7	5.69
	2	2	4	631	22.7	5.68
	4	4	8	630	22.7	5.67
	8	8	16	629	22.6	5.66
Large (14.35 nm)	1	1	2	5780	208	52.0
	2	2	4	5810	209	52.3
	4	4	8	5870	211	52.8
	8	8	16	5940	214	53.4

Hydrodynamic radii of each species are indicated in parentheses.

References

1 B. K. Johnson and R. K. Prud'homme, *Australian Journal of Chemistry*, 2003, **56**, 1021–1024.

2 B. K. Johnson and R. K. Prud'homme, *AIChE Journal*, 2003, **49**, 2264–2282.